

This version of the article has been accepted for publication, after a peer-review process, and is subject to Springer Nature's AM terms of use, but is not the Version of Record and does not reflect post-acceptance improvements, or any corrections. The Version of Record is available online at: <https://doi.org/10.1007/s10915-016-0188-7>

High order weighted extrapolation for boundary conditions for finite difference methods on complex domains with Cartesian meshes

A. Baeza · P. Mulet · D. Zorío

Abstract The design of numerical boundary conditions is a challenging problem that has been tackled in different ways depending on the nature of the problem and the numerical scheme used to solve it. In this paper we present a new weighted extrapolation technique which entails an improvement with respect to the technique that was developed in [1]. This technique is based on the application of a variant of the Lagrange extrapolation through the computation of weights capable of detecting regions with discontinuities. We also present a combination of the above technique with a least squares approach in order to stabilize the scheme in some cases where Lagrange extrapolation can turn the scheme mildly unstable. We show that this combined extrapolation technique can tackle discontinuities more robustly than the procedure introduced in [1].

Keywords Finite difference WENO schemes, Cartesian grids, weighted extrapolation.

1 Introduction

There are many physical phenomena that are described by hyperbolic conservation laws. The lack of knowledge about the analytic solution of most of them motivated the development of numerical methods to approximate their solutions in the last decades.

In order to solve them accurately, the schemes evolved to improve the accuracy and to capture well the discontinuities in weak solutions. Due either to the nature of the problems or to the impossibility of handling unbounded domains on a computer numerical boundary conditions have to be imposed.

Despite high order numerical methods have been widely studied and developed, usually the boundary treatment has consisted in low order extrapolations, decreasing the global order of the scheme and the quality of the simulation results.

In this paper we present a weighted extrapolation technique for the application of numerical boundary conditions in numerical schemes using Cartesian meshes,

Departament de Matemàtica Aplicada, Universitat de València (Spain); emails: antonio.baeza@uv.es, mulet@uv.es, david.zorio@uv.es. This research was partially supported by Spanish MINECO grants MTM2011-22741 and MTM2014-54388-P.

which represents an improvement of our previous work [1], where a Boolean node selection with a thresholding criterion was used. In this paper we will design a fully weighted boundary extrapolation, with scale independent and dimensionless weights. We will combine these techniques with a least squares extrapolation to overcome some stability issues that may appear in some smooth problems with complex boundary shape.

This work can be understood as an extension to a higher order of accuracy of [11], where second order Lagrange extrapolation with slope limiters is used to extrapolate to a single ghost cell. A related approach for data extrapolation at the boundary with high order is proposed in [12] and [13], where the authors develop an extrapolation technique for inflow boundaries (known as inverse Lax-Wendroff) which is based on using the equations to compute normal derivatives and approximate ghost values by means of a Taylor expansion that involves the Dirichlet boundary conditions and the computed derivatives, whereas ghost cell values at outflow boundaries are approximated by means of combinations of Lagrange and WENO extrapolation and least-squares approximation. The aforementioned technique relies on weights that are not adimensional and scale dependent. Later on, the authors of [6] introduced a modification that overcame the dependency on the scale.

The organization of the paper is the following: In section 2 we present the equations and the numerical methods that we consider in this paper. The details of the procedure for meshing complex domains with Cartesian meshes are explained in section 3, where we also expound how we perform extrapolations at the boundary. In section 4 we present a proposal for weighted extrapolation and introduce several procedures that can be used to design the weights. Some numerical results that are obtained with this methodology are presented in section 5, with some simple tests in 1D to illustrate the correct behavior of the proposed techniques and some more complex ones in 2D. Finally, some conclusions are drawn in section 6.

2 Numerical scheme

We will consider along this paper hyperbolic systems of m two-dimensional conservation laws

$$u_t + f(u)_x + g(u)_y = 0, \quad u = u(x, y, t), \quad (1)$$

defined on an open and bounded spatial domain $\Omega \subseteq \mathbb{R}^2$, with Lipschitz boundary $\partial\Omega$, a finite union of piece-wise smooth curves, $u : \Omega \times \mathbb{R}^+ \rightarrow \mathbb{R}^m$, and fluxes $f, g : \mathbb{R}^m \rightarrow \mathbb{R}^m$. These equations are supplemented with an initial condition, $u(x, y, 0) = u_0(x, y)$, $u_0 : \Omega \rightarrow \mathbb{R}^m$, and different boundary conditions that may vary depending on the problem.

The techniques that will be expounded in this paper can be used in a more general family of numerical schemes; however, we use here Shu-Osher's finite difference conservative methods [10] with a WENO5 (*Weighted Essentially Non-Oscillatory*) [7] spatial reconstruction, Donat-Marquina's flux-splitting [5] and the RK3-TVD ODE solver [9]. This combination of techniques was proposed in [8].

3 Meshing procedure

The mesh is defined through the following items: a reference vertical line, $x = \bar{x}$, a horizontal line $y = \bar{y}$ and two positive values $h_x > 0$ and $h_y > 0$, the horizontal and vertical spacings of the mesh, so that the vertical lines in the mesh are determined by: $x = x_r := \bar{x} + rh_x$, $r \in \mathbb{Z}$ and the horizontal ones by $y = y_s := \bar{y} + sh_y$, $s \in \mathbb{Z}$. The computational domain is given by the intersections of the horizontal and vertical mesh lines that belong to the physical domain:

$$\mathcal{D} := \{(x_r, y_s) : (x_r, y_s) \in \Omega, \quad r, s \in \mathbb{Z}\} = (\bar{x} + h_x \mathbb{Z}) \times (\bar{y} + h_y \mathbb{Z}) \cap \Omega.$$

Each point (x_r, y_s) determines a rectangular cell by:

$$\left[x_r - \frac{h_x}{2}, x_r + \frac{h_x}{2}\right] \times \left[y_s - \frac{h_y}{2}, y_s + \frac{h_y}{2}\right].$$

In order to advance in time using WENO schemes of order $2k - 1$, k additional cells are needed at both sides of each horizontal and vertical mesh line. If these additional cells fall outside the domain they are usually named *ghost cells* and, in terms of their centers, are given by:

$$\mathcal{GC} := \mathcal{GC}_x \cup \mathcal{GC}_y,$$

where

$$\mathcal{GC}_x := \{(x_r, y_s) : 0 < d(x_r, \Pi_x(\mathcal{D} \cap (\mathbb{R} \times \{y_s\}))) \leq kh_x, \quad r, s \in \mathbb{Z}\},$$

$$\mathcal{GC}_y := \{(x_r, y_s) : 0 < d(y_s, \Pi_y(\mathcal{D} \cap (\{x_r\} \times \mathbb{R}))) \leq kh_y, \quad r, s \in \mathbb{Z}\},$$

with Π_x and Π_y being the projections on the respective coordinates and,

$$d(a, B) := \inf\{|b - a| : b \in B\},$$

for given $a \in \mathbb{R}$ and $B \subseteq \mathbb{R}$. Notice that $d(a, \emptyset) = +\infty$, since, by convention, $\inf \emptyset = +\infty$.

There are many ways to compute the ghost cell values that are required for the numerical scheme to advance in time. In order to maintain the accuracy and stability of the numerical method many issues are to be taken into account.

First of all and regarding the node organization and selection it seems reasonable to use the lines normal to the boundary as directions for extrapolation, since many physical boundary conditions (e.g. Dirichlet) use the normal lines in their definition. It seems thus reasonable that the extrapolation at a certain ghost cell P be based on the physical conditions at its nearest boundary point, P_0 , a solution of

$$\|P - P_0\|_2 = \min\{\|P - B\|_2 : B \in \partial\Omega\}.$$

Uniqueness of P_0 holds whenever P is close enough to the boundary, so we will henceforth denote $N(P) = P_0$. The line determined by P and $N(P)$ is the line normal to $\partial\Omega$ at $N(P)$ if $\partial\Omega$ is differentiable at P_0 . In a general setting nodes inside the domain do not fall along boundary normals and therefore a prior interpolation process is to be made at some nodes lying at the normal. For simplicity we will not distinguish between interpolation or extrapolation, and the second term will be routinely used for both procedures. The motivation of the choice of the nodal

disposition that we will introduce next and further details about it can be found in [1].

If a numerical scheme of order $r + 1$ is used to numerically solve the equations and we wish to design a procedure for numerical boundary conditions that formally preserve the accuracy in the resulting scheme it is reasonable to use extrapolation of the same order as the numerical method (or higher) at the ghost cells.

We proceed in a similar fashion as in [11] and [1]. Given $P \in \mathcal{GC}$ and $R \geq r$ we build a set of points $\mathcal{N}(P) = \{N_1, \dots, N_{R+1}\}$ by first selecting the horizontal or vertical direction and considering the first $R + 1$ interior intersections of the line determined by P and $\mathcal{N}(P)$ with the mesh lines corresponding to the selected direction. The choice of one direction or the other depends on the slope of the normal line, so that the use of interior information is maximized. Figure 1 illustrates this approach.

Let us remark that in [1] the spacing of the nodes at the normal lines used for extrapolation was forced to be not smaller than the distance between the ghost cell and the boundary cell that defined the normal line. The reason was that for linear (first order) extrapolation stability issues appear if that constraint is not fulfilled. Numerical experimentation shows that for higher order extrapolation there are no stability issues if the nodes (including the boundary condition, if any), are separated between them a distance not smaller than the mesh size, regardless of the position of the ghost cell. This results on a more accurate approximation as the node spacing is smaller in this case.

We denote by $v = (v_1, v_2)$ the vector determined by P and $\mathcal{N}(P)$, and $\mathcal{S}_q = \{N_{q,1}, \dots, N_{q,R+1}\}$ the closest set of points to N_q from the computational domain sharing the same coordinate than N_q , this depending on the angle of the normal line as explained in [1]. Using the 1D stencil \mathcal{S}_q an approximation of the numerical solution at N_q is computed by the same means used for extrapolation at the ghost cell, described in Section 4.

Since we are now concerned on performing a weighted extrapolation and the computation of smoothness indicators to build the weights can be very computationally expensive if the data is not equally spaced, as it will generally happen on Dirichlet boundaries, we perform an additional step before extrapolating the value at the ghost cell in order to generate a new stencil that includes the boundary node and is composed by equally spaced points.

Therefore, if Dirichlet conditions are prescribed, we use the data obtained in N_q , $1 \leq q \leq R + 1$ to perform 1D interpolations at the points P_q , $1 \leq q \leq R$, where $P_q = (P_0^x + qh_x, P_0^y + q\frac{v_2}{v_1}h_x)$, $0 \leq q \leq R$ if $|v_1| \geq |v_2|$ or $P_q = (P_0^x + q\frac{v_1}{v_2}h_y, P_0^y + qh_y)$, $0 \leq q \leq R$, otherwise, and use the data from the stencil $\mathcal{S}(P) = \{P_0, P_1, \dots, P_R\}$ to extrapolate it at the ghost cell P .

In case of outflow conditions, we extrapolate directly the data from the stencil $\mathcal{S}(P) = \{N_1, N_2, \dots, N_{R+1}\}$. See Figure 1 for graphical examples.

If the boundary does not change with time the elements involved in the computation of the extrapolated value at P are determined only once at the beginning of the simulation.

Summarizing, the complete extrapolation procedure is done in two stages in the case of outflow boundaries and in three in the case of Dirichlet boundaries: in a first step data located at the normal lines is computed from the numerical solution by (horizontal or vertical) 1D interpolation; in the second one, only performed on Dirichlet boundaries, the nodes obtained in the first step are used to interpolate

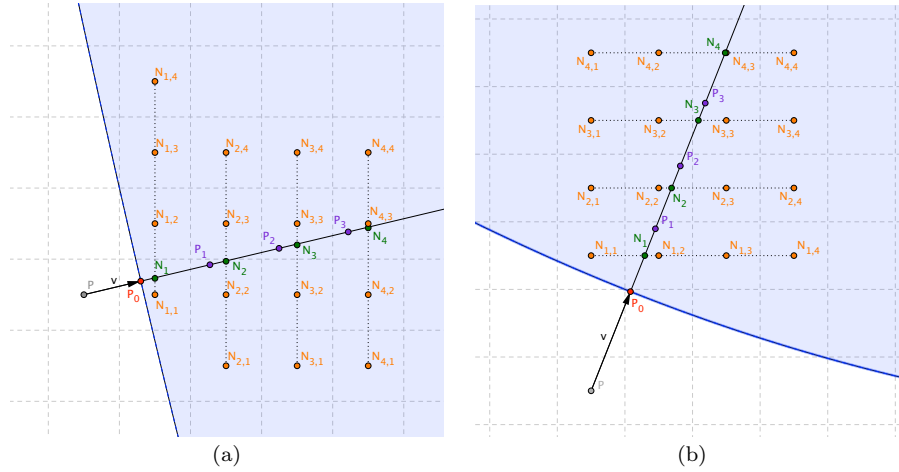


Fig. 1: Examples of choice of stencil. We use the stencil $S(P) = \{N_1, N_2, N_3, N_4\}$ in case of outflow boundary and conditions and the stencil $S(P) = \{P_0, P_1, P_2, P_3\}$ in case of Dirichlet boundary conditions.

at new points at the normal line so that they compose an equally spaced stencil together with the point $N(P)$; finally, values for the ghost cell are obtained by 1D extrapolation along the normal line obtained in the first stage (in case of outflow boundary) or the second stage (in case of Dirichlet boundary). Note that stencils with equally spaced nodes are used in all the above approximations.

We next introduce an extrapolation procedure that takes into account the potential presence of discontinuities in the numerical solution.

4 Extrapolation

As stated in [1], special care must be taken when performing extrapolation at the boundary mainly due to the potential lack of regularity in the solution and to the stability restrictions induced by small-cut cells. It was also seen there that the classical ENO and WENO methods are not suitable for this task and a new technique that overcame the above issue was developed. The method was based on a Boolean criterion for the selection of the nodes that ultimately compose the stencil used to extrapolate. A decision on whether a candidate node was added to the stencil or discarded was made through an smoothness analysis and controlled via threshold values. The method produces high order extrapolations when the solution is smooth and takes into account the possible presence of discontinuities.

We now present a new technique, which can be considered as an evolution of the thresholding method, based on the computation of dimensionless and scale independent weights that outperforms the aforementioned method and depends on less parameters.

4.1 Weighted extrapolation

Consider a stencil of not necessarily equally nodes $x_0 < \dots < x_r$ and their corresponding nodal values $u_j = u(x_j)$. Denote $J = \{0, \dots, r\}$ and $X = \{x_j\}_{j \in J}$ and let x_* be the node where we wish to interpolate and j_0 the interior node which is closest to x_* , i. e.,

$$j_0 = \operatorname{argmin}_{j \in J} |x_j - x_*|.$$

The goal is to approximate the value that x_* should have, based on the information of the “smoothest” substencil and the node x_{j_0} . We define inductively the following set of indexes:

$$J_0 = \{j_0\}, \text{ and } X_0 = \{x_j\}_{j \in J_0} = \{x_{j_0}\}$$

Assume we have defined J_{k-1} , then J_k is defined by

$$J_k = J_{k-1} \cup \{j_k\} \text{ and } X_k = \{x_j\}_{j \in J_k}$$

where

$$x_{j_k} = \operatorname{argmin}_{j \in J \setminus J_{k-1}} |x_j - x_*|.$$

That is, we add the closest node to x_* from the remaining nodes to choose as we increase k . X_k and J_k can be defined for $0 \leq k \leq r$.

By construction, it is clear that the set X_k can be written as a sequence of nodes with successive indexes, i.e., stencils:

$$X_k = \{x_{i_k+j}\}_{j=0}^k$$

for some $0 \leq i_k \leq r - k$, $0 \leq k \leq r$.

Now, for each k , $0 \leq k \leq r$, we define p_k as the interpolating polynomial of degree at most k such that $p_k(x_{i_k+j}) = u_{i_k+j}$, $\forall j, 0 \leq j \leq k$. Given a set of weights $\{\omega_k\}_{k=1}^r$ such that $0 \leq \omega_k \leq 1$, we define the following recurrence:

$$\begin{aligned} u_*^{(0)} &= p_0(x_*) = u_{i_0}, \\ u_*^{(k)} &= (1 - \omega_k)u_*^{(k-1)} + \omega_k p_k(x_*), \quad 1 \leq k \leq r. \end{aligned} \tag{2}$$

We define the final result of the weighted extrapolation as

$$u_* := u_*^{(r)},$$

which will be taken as an approximation for the value $u(x_*)$.

The idea is to increase the degree of the interpolating polynomial only if the solution in the corresponding stencil is smooth, and therefore the chosen weights should verify that $\omega_k \approx 0$ if the stencil J_k crosses a discontinuity and $\omega_k \approx 1$ if the data from the stencil is smooth. We will show below a weight construction that verifies that property as well as the capability of preserving the accuracy order of the extrapolation in case of smoothness.

From now on, we will assume that the nodes X are equally spaced and define $h = x_{j+1} - x_j$.

For each $1 \leq k \leq r$, we define a slight modification of the Jiang-Shu smoothness indicator [7] associated to the stencil J_k as the following value:

$$I_k = \frac{1}{r} \sum_{\ell=1}^k \int_{x_0}^{x_r} h^{2\ell-1} p_k^{(\ell)}(x)^2 dx.$$

Now, given $1 \leq r_0 \leq E\left(\frac{r}{2}\right)$, where $E(x) = \max \mathbb{Z} \cap (-\infty, x]$, we will seek for a smoothness zone along the stencils of $r_0 + 1$ points as a reference.

This procedure will work correctly if there is only one discontinuity in the stencil, and the restriction $r_0 \leq E\left(\frac{r}{2}\right)$ is set in order to avoid a stencil overlapping, since a discontinuity might eventually be in the overlapping zone and thus none of the stencils would include smooth data. Define

$$IS_k = \min_{0 \leq j \leq r-k} \frac{1}{r} \sum_{\ell=1}^{r_0} \int_{x_0}^{x_r} h^{2\ell-1} q_{k,j}^{(\ell)}(x)^2 dx, \quad 1 \leq k \leq r_0,$$

where $q_{k,j}$ is the polynomial of degree at most k such that $q_{k,j}(x_{j+i}) = u_{j+i}$ for $0 \leq i \leq k$, $0 \leq j \leq r-k$.

There are many possibilities for defining the weights in (2). We next introduce several possibilities that might be suitable for different scenarios. We start with two designs that we name Simple Weights (SW) and Improved Weights (IW) that show good performance for problems that have smooth solutions but might misbehave otherwise. Albeit the interest of such approaches is reduced to academic problems we describe them in sections 4.2 and 4.3 with some detail as they are illustrative of the ideas behind other methods described in the rest of the section, which are much more oriented to more challenging problems that may include the typical non-smooth features of hyperbolic problems.

Numerical experimentation shows that the use of the SW and IW methods in complex problems can lead to poor results, probably because of the low numerical viscosity introduced by the methods at the boundary. For this reason, we introduce new weight designs which are derived from the two aforementioned extrapolation techniques. These are the unique weight (UW), where the extrapolation is performed by computing one weight, a tuned version (λ -UW), where the tuning parameter λ can magnetize the weight to 0 or 1 in order to improve the quality of the extrapolation depending on the context we are working in, and the global average weight (GAW), also based on a single weight, but more robust than the UW version.

Finally, since some stability issues may appear if the extrapolation is solely based on Lagrange extrapolation, we introduce a least-squares extrapolation procedure, which can be ultimately combined with any of the the weighted extrapolation techniques. We refer to this combination as Weighted Least Squares (WLS) so that WLS-X denotes the WLS technique combined with weights computed by method X.

4.2 Simple weights (SW)

The weights are defined as follows

$$\begin{aligned}\omega_k &= 1 - \left(1 - \left(\frac{IS_k}{I_k}\right)^{s_1}\right)^{s_2}, \quad 1 \leq k \leq r_0, \\ \omega_k &= \min \left\{1 - \left(1 - \left(\frac{IS_{r_0}}{I_k}\right)^{s_1}\right)^{s_2}, 1\right\}, \quad r_0 + 1 \leq k \leq r.\end{aligned}\tag{3}$$

A small positive number $\varepsilon > 0$ is added to each smoothness indicator in order to avoid the denominator to become zero (in all our experiments, we take $\varepsilon = 10^{-100}$). The parameter s_1 enforces the convergence to 0 when the stencil is not smooth, while the parameter s_2 enforces the convergence to 1 when it is smooth.

It can be shown that for a smooth stencil, if there exists some $1 \leq k_0 \leq r_0$ such that $|u^{(k_0)}| \gg 0$ around the stencil, then

$$\omega_k = 1 - \mathcal{O}(h^{s_2})$$

and if the stencil crosses a discontinuity, then

$$\omega_k = \mathcal{O}(h^{2s_1}).$$

A drawback of this weight design, apart from the loss of accuracy when all the k -th derivatives $1 \leq k \leq r_0$ vanish near the stencil, is the fact that sometimes the optimal order cannot be attained regardless of the values of s_1 and s_2 . Consider for instance $r = 5$ and $r_0 = 2$ and the function

$$u(x) = \begin{cases} x^2, & x \leq 0 \\ 1, & x > 0 \end{cases}$$

Now we take the nodes $x_i = -0.5 + 0.2i$, $0 \leq i \leq 5$ and the corresponding values u_i are $U = \{0.25, 0.09, 0.01, 1, 1, 1\}$. Since one of the substencils of three points contains $\{1, 1, 1\}$, it is clear then that $IS = 0$ and therefore $\omega_k = 0$, $\forall k$, $1 \leq k \leq 5$. If we performed a weighted extrapolation to $x_* = -0.7$ then it would be obtained the nodal value from the corresponding closest node, $x_0 = -0.5$, that is, $u_* = u_0 = 0.25$, while the most reasonable thing to do would be to perform a second order extrapolation taking the first three nodes (take all the nodes from the correct side of the discontinuity), which gives 0.49. The aforementioned scenario is depicted in Figure 2.

This has occurred because in this case the smoothest substencil belongs to the other side of the discontinuity, and thus the information about the derivatives is wrong. We next present an alternative weight design that overcomes the above issue.

4.3 Improved weights (IW)

The previously mentioned issue can be solved through the following modification of the weights design. In this new weight design we will define and combine additional parameters in order to ensure that, for stencils with discontinuities, the

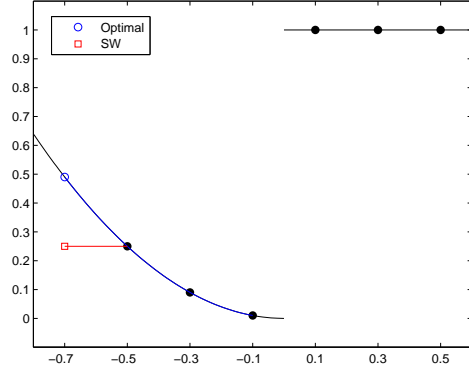


Fig. 2: Comparison of the SW extrapolation results against the expected optimal result.

information is taken from the correct side of the discontinuity. Let us now consider the maximum value of the up to r_0 -th order smoothness indicators:

$$IM_k = \max_{0 \leq j \leq r-k} \frac{1}{r} \sum_{\ell=1}^{r_0} \int_{x_0}^{x_r} h^{2\ell-1} q_{k,j}^{(\ell)}(x)^2 dx, \quad 1 \leq k \leq r_0.$$

We define

$$\sigma_k := \min \left\{ \frac{IS_{\min\{k, r_0\}}}{I_k}, 1 \right\},$$

$$\tau_k := \frac{I_k}{IM_k},$$

and

$$\rho_k = \tau_k \left(\frac{1 - \sigma_k}{\sigma_k} \right)^d, \quad d \geq \frac{r}{2},$$

to finally define our new weights as

$$\omega_k = \frac{1}{1 + \rho_k}. \quad (4)$$

We now see in detail the reason for this choice. These are the possible values in terms of powers of $\mathcal{O}(h)$ that both quotients between smoothness indicators can take:

$$\sigma_k = \begin{cases} 1 - \mathcal{O}(h) & \text{if there is smoothness,} \\ \mathcal{O}(h^2) & \text{if } X_k \text{ crosses a discontinuity.} \end{cases}$$

However, if there is not smoothness but still X_k does not cross a discontinuity there may be two possibilities: $IS_{\min\{k, r_0\}}$ is obtained in the “correct” side or in the “wrong” one. In the first case, we would have $\frac{IS_{\min\{k, r_0\}}}{I_k} = 1 + \mathcal{O}(h)$, as desired, but otherwise, if the derivatives are different from one side and another in

a random fashion, that would lead to quotients with values in a random fashion as well. Here is thus the importance of the second quotient in order to fix such issue:

$$\tau_k = \begin{cases} 1 + \mathcal{O}(h) & \text{if there is smoothness,} \\ \mathcal{O}(h^2) & \text{if there is not smoothness and } X_k \text{ belongs to a smooth zone,} \\ \mathcal{O}(1) & \text{if there is not smoothness and } X_k \text{ crosses a discontinuity,} \end{cases}$$

where $\mathcal{O}(1)$ means that it is a value comprised between 0 and 1 in a random fashion, but not $\mathcal{O}(h)$ since in that case it is a quotient between two smoothness indicators, both in non-smooth zones. Note from that the term IM_k from the definition of τ_k can be replaced by I_r , since in this case τ will still verify the above properties and less smoothness indicators will be required to be computed. In practice, we will work through this modification.

One can show that this way

$$\rho_k = \begin{cases} \mathcal{O}(h^d) & \text{if } X_k \text{ belongs to a smooth zone,} \\ \mathcal{O}(h^{-2d}) & \text{if } X_k \text{ crosses a discontinuity,} \end{cases}$$

as desired, and thus

$$\omega_k = \begin{cases} 1 - \mathcal{O}(h^d) & \text{if } X_k \text{ belongs to a smooth zone,} \\ \mathcal{O}(h^{2d}) & \text{if } X_k \text{ crosses a discontinuity,} \end{cases}$$

except when all derivatives up to the r_0 -th one are close to be zero in some of the two discontinuity sides, where the value of the weight cannot be predicted, although it will take values more likely close to 0 rather than 1.

We can fix this issue by redefining σ_k as

$$\sigma_k = \frac{IS_k + \beta}{I_k + \beta}, \quad (5)$$

where β is assumed to be a small quantity, $\beta = \mathcal{O}(h^b)$, $b \leq 2r_0$. We propose two different choices of β satisfying that condition:

- $\beta = \lambda^2 h^{2r_0}$, where λ is a parameter proportional to the scaling of the solution. That is, if we re-scale the data by a factor of μ , then the value λ should be replaced by $\mu\lambda$.
- In our context, we have knowledge about a wide range of point values of a function (the numerical data from a computational domain in a certain scheme). Hence, we can naturally define a quantity $\mathcal{O}(h^{2r_0})$ depending directly on the data of the problem.

For instance, if we assume we have a 1D simulation with data U_j , $0 \leq j \leq n$, then one can define

$$\beta = \left(\frac{1}{n} \sum_{j=1}^n |u_j - u_{j-1}| \right)^{2r_0} = TV(u)^{2r_0} h^{2r_0}.$$

The above value can be generalized to any dimension as a global average of all the absolute values of all the directional undivided differences (in all directions). When discontinuities and zeros at the first derivative are supposed to be in a region of measure 0, the above value verifies $\beta = \mathcal{O}(h^{2r_0})$, while keeping σ_k scaling independent. This argument is also valid even when the first derivative

is zero almost everywhere, but there is a discontinuity on the data, which is also a common case as initial condition for shock problems. Another valid case is when, despite having zeros in the derivative in a non-null region, there is a non-null region having non-zero derivatives as well provided that the discontinuities, if any, are located in a null region.

If one wants to keep some stricter control of the above parameter due to the presence of very strong discontinuities which might make β too big, one can always consider a tuning parameter κ (in this case independent of the scaling as well) and redefine σ_k as

$$\sigma_k = \frac{IS_k + \kappa\beta}{I_k + \kappa\beta}.$$

If one uses the above technique to avoid a loss of accuracy near zeros on the corresponding derivatives and makes sure that the parameters, if any, are well tuned, it makes no sense to use a smoothness control stencil longer than a two-points one, and thus for that case we will always use $r_0 = 1$. Moreover, in this particular case it is no longer needed to define σ_k such that does not surpass the unity, since we have the following result.

Property 1 *If $r_0 = 1$ then*

$$\alpha_k := \frac{I_1}{I_k}$$

verifies $0 \leq \alpha_k \leq 1$, $1 \leq k \leq r$.

Proof Given $f, g \in L^2([x_{i-1}, x_i])$ we define the following scalar products

$$\langle f, g \rangle_i = \int_{x_{i-1}}^{x_i} f(x)g(x)dx$$

and their induced norms as

$$\|f\|_i^2 = \langle f, f \rangle_i, \quad 1 \leq i \leq r.$$

Now, taking into account that $x_i - x_{i-1} = h$, we have

$$\begin{aligned} I_k &= \frac{1}{r} \sum_{\ell=1}^k \int_{x_0}^{x_r} h^{2\ell-1} p_k^{(\ell)}(x)^2 dx \geq \frac{1}{r} \int_{x_0}^{x_r} h p_k'(x)^2 dx = \frac{1}{r} \sum_{i=1}^r h \int_{x_{i-1}}^{x_i} p_k'(x)^2 dx \\ &= \frac{1}{r} \sum_{i=1}^r \int_{x_{i-1}}^{x_i} dx \int_{x_{i-1}}^{x_i} p_k'(x)^2 dx = \frac{1}{r} \sum_{i=1}^r \|f_i\|_i^2 \|g_i\|_i^2, \end{aligned}$$

where $f_i(x) = 1$ and $g_i(x) = p_k'(x)$ for $x \in [x_{i-1}, x_i]$. By the Cauchy-Schwarz Inequality

$$\langle f_i, g_i \rangle_i^2 \leq \|f_i\|_i^2 \|g_i\|_i^2$$

we have

$$\begin{aligned} I_k &\geq \frac{1}{r} \sum_{i=1}^r \|f_i\|_i^2 \|g_i\|_i^2 \geq \frac{1}{r} \sum_{i=1}^r \langle f_i, g_i \rangle_i^2 = \frac{1}{r} \sum_{i=1}^r \left(\int_{x_{i-1}}^{x_i} f_i(x)g_i(x)dx \right)^2 \\ &= \frac{1}{r} \sum_{i=1}^r \left(\int_{x_{i-1}}^{x_i} p_k'(x)dx \right)^2 = \frac{1}{r} \sum_{i=1}^r (p_k(x_i) - p_k(x_{i-1}))^2 = \frac{1}{r} \sum_{i=1}^r (u_i - u_{i-1})^2 \\ &\geq \frac{1}{r} \sum_{i=1}^r \min_{1 \leq j \leq r} (u_j - u_{j-1})^2 = \min_{1 \leq j \leq r} (u_j - u_{j-1})^2 = I_1. \end{aligned}$$

□

With these modifications, weighted extrapolation will not suffer from a loss of accuracy in any case and it will have the optimal order in presence of sharp discontinuities.

If we now apply this technique, it will still capture well sharp discontinuities while keeping the highest order as possible when there is a discontinuity in the stencil.

4.4 Examples

Example 1. Let $u : \mathbb{R} \rightarrow \mathbb{R}$ a function defined by

$$u(x) = \begin{cases} x^2 & \text{if } x \leq 1, \\ 1 + x^3 & \text{if } x > 1. \end{cases}$$

We study numerically the accuracy behavior of our scheme in a six points stencil around the discontinuity point $x = 1$ when $h \rightarrow 0$. Given $h > 0$ we select as stencil the set of nodes $x_i = 1 + (-2.5 + i)h$, $0 \leq i \leq 5$. Figure 3 shows a graphical example of the grid points for $h = 0.2$ and $h = 0.1$.

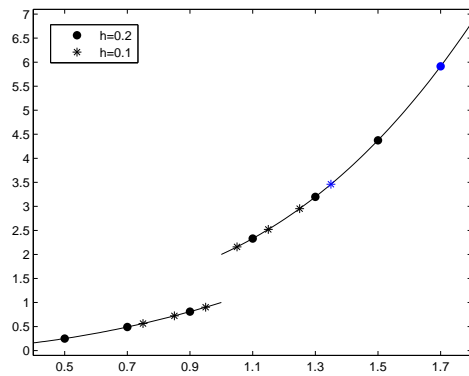


Fig. 3: Illustration of the grid configuration in Example 1.

We start with $h_0 = 0.04$ and define $h_i = h_{i-1}/2$ for $1 \leq i \leq 6$ and compute the exact errors extrapolating at $x_* = 1 + 3.5h$ using the above techniques. A successful one should give third order accuracy since there are available three points from the right side of the discontinuity.

The results obtained with the simple weights (3) for $s_1 = s_2 = 3$ and $r_0 = 2$ are shown in Table 1.

It can be clearly seen that the optimal accuracy is not attained by this weight design.

The technical reason for this happening is that the derivative of u for $x \neq 1$ is

$$u'(x) = \begin{cases} 2x & \text{if } x < 1, \\ 3x^2 & \text{if } x > 1, \end{cases}$$

Resolution	Error	Order
h_0	5.72E-2	–
h_1	1.18E-2	1.48
h_2	7.40E-3	1.32
h_3	3.24E-3	1.19
h_4	1.51E-3	1.10
h_5	7.26E-4	1.06
h_6	3.56E-4	1.03

Table 1: Simple weights (3), example 1.

and thus $\lim_{x \rightarrow 1^-} u'(x) = 2$ and $\lim_{x \rightarrow 1^+} u'(x) = 3$, hence since the “smoothest” information is taken from the left side of the discontinuity but the actual information should be taken from the right side of the discontinuity, where there is smoothness as well. Therefore, the weights ω_k , $1 \leq k \leq 2$, converge to $(1 - (\frac{2}{3})^3)^3$ as $h \rightarrow 0$ rather than 1 for the above explained reason.

Now, we repeat the same test using the new weights defined in (4) for $d = 3$ and $r_0 = 1$ and we present in Table 2 the errors for the same setup as above, where it can be clearly seen that the optimal third order accuracy is obtained.

Resolution	Error	Order
h_0	3.89E-4	–
h_1	4.82E-5	3.01
h_2	6.01E-6	3.00
h_3	7.50E-7	3.00
h_4	9.38E-8	3.00
h_5	1.17E-8	3.00
h_6	1.46E-9	3.00

Table 2: Improved weights (4), example 1.

Example 2. We now consider an example where one derivative vanishes. This example is very similar to the one presented to motivate the definition of the improved weights. In this case, we define $u : \mathbb{R} \rightarrow \mathbb{R}$ as

$$u(x) = \begin{cases} \sin(x) & \text{if } x \leq 0, \\ 1 & \text{if } x > 0. \end{cases}$$

We define now the grid points as $x_i = (-2.5 + i)h$, $0 \leq i \leq 5$, whose configuration is depicted in Figure 4 for $h = 0.2$ and $h = 0.1$.

Taking the same values of h as in the above experiment, we now extrapolate at $x_* = -3.5h$ and we obtain the results in Table 3 using the improved weights with the same parameters as above. This order decay is now due to the fact that one of the derivatives vanishes.

To fix this, we use the weight modification suggested in (5) by taking $\beta = h^2$, obtaining third order accuracy as can be observed in table 4.

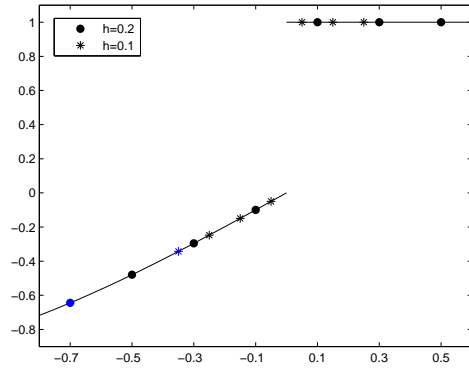


Fig. 4: Illustration of the grid configuration in Example 2.

Resolution	Error	Order
h_0	3.97E-2	—
h_1	2.00E-2	0.99
h_2	1.00E-2	1.00
h_3	5.00E-3	1.00
h_4	2.50E-3	1.00
h_5	1.25E-3	1.00
h_6	6.25E-4	1.00

Table 3: Improved weights (4), example 2.

Resolution	Error	Order
h_0	6.38E-4	—
h_1	7.99E-5	3.00
h_2	1.00E-5	3.00
h_3	1.25E-6	3.00
h_4	1.56E-7	3.00
h_5	1.95E-8	3.00
h_6	2.44E-9	3.00

Table 4: Improved weights (4), $\beta = h^2$, example 2.

4.5 Unique weight extrapolation (UW)

In this section we propose a method that uses only one weight to decide the extrapolation method attending to the global smoothness in the stencil X that contains all $r+1$ nodes. The idea is that switching to a low order reconstruction as soon as a lack of smoothness is detected increases the robustness of the procedure in the non-smooth case when the extrapolation is performed in the context of PDEs, where discontinuities get smeared, while maintaining high order in the smooth case, besides being more computationally efficient.

As our purpose, apart from achieving robustness, is also designing an efficient method, we will propose for the UW method a simplified version of the smoothness indicators introduced previously. We will also introduce in Section 4.5.1 an additional (and optional) tuning parameter, with which we can map the original weight ω to another one through a transformation that magnetizes values far from

1 (but still far from 0 as well) to 0. This variant is particularly useful in problems with strong shocks –as in this case the weights should be very close to 0– or in problems with complex smooth structure –where the results are better if the weights are close to 1 near them–.

The computation of the weights in the previous cases implies the use of logical structures since a minimum has to be computed. We overcome this issue as well by designing a weight capable of capturing well the discontinuities while keeping high order accuracy on smooth zones. This will be discussed in section 4.5.2.

The procedure for the extrapolation with only one weight is performed in the following sense: Instead of gradually increasing the degree of the interpolating polynomials, we will just average the constant extrapolation ($k = 0$) and maximum degree extrapolation ($k = r$), that is, we will consider

$$u_* = (1 - \omega)p_0(x_*) + \omega p_r(x_*) = (1 - \omega)u_{i_0} + \omega p_r(x_*),$$

where

$$\omega = \min \left\{ 1 - \left(1 - \left(\frac{IS_{r_0}}{I_r} \right)^{s_1} \right)^{s_2}, 1 \right\}.$$

It can be shown that for a smooth stencil, if there exists some $1 \leq k_0 \leq r_0$ such that $|u^{(k_0)}| \gg 0$ around the stencil, then

$$\omega = 1 - \mathcal{O}(h^{s_2})$$

and if the stencil crosses a discontinuity, then

$$\omega = \mathcal{O}(h^{2s_1}).$$

In order to lower the computational cost and ensure that $0 \leq \omega \leq 1$ without having to artificially bound it by 1 when $r_0 > 1$, we can replace the definition of I_r , which is a smoothness indicator of the whole $r + 1$ points stencil, by the average of all smoothness indicators of the substencils of $r_0 + 1$ points, i.e.:

$$I_r^* := \frac{1}{r - r_0 + 1} \sum_{j=0}^{r-r_0} I_{r_0,j},$$

where

$$I_{r_0,j} = \frac{1}{r_0} \sum_{\ell=1}^{r_0} \int_{x_j}^{x_{r_0+j}} h^{2\ell-1} q_{r_0,j}^{(\ell)}(x)^2 dx. \quad (6)$$

Then one can define

$$\omega = 1 - \left(1 - \left(\frac{IS_{r_0}}{I_r^*} \right)^{s_1} \right)^{s_2},$$

which in this case it clearly verifies $0 \leq \omega \leq 1$.

Under the hypothesis $\exists k_0 \in \mathbb{N}$, $1 \leq k_0 \leq r_0$ such that $|u^{(k_0)}| \gg 0$ around the stencil, then

$$u_* = u(x^*) + \mathcal{O}(h^{r'+1}),$$

where $r' = \min\{s_2(r_0 - k_0 + 1), r\}$.

4.5.1 Tuned weight (λ -UW)

When the stencil includes globally some smeared discontinuity, one can map a ω value such that $\omega \gg 0$ and $\omega \ll 1$ to a new one $\tilde{\omega} \approx 0$, as desired in this case, but that at same time $\tilde{\omega} \approx 1$ when $\omega \approx 1$ as well.

Let $\tilde{\omega} = F_\lambda(\omega)$ be

$$\tilde{\omega} := \begin{cases} \frac{e^{\lambda\omega} - 1}{e^\lambda - 1} & \text{if } \lambda \neq 0 \\ \omega & \text{if } \lambda = 0 \end{cases},$$

for some $\lambda \in \mathbb{R}$. It can be proven that $\forall \omega \in [0, 1]$, $G_\omega \in C^\infty(\mathbb{R})$, where $G_\omega(\lambda) := F_\lambda(\omega)$. The larger λ is, the stricter the discontinuity detection filter will be. The lower (negative) λ is, the more permissive it will be.

Assume smoothness conditions, therefore $\omega = 1 - \delta$, where $\delta = \mathcal{O}(h^{s_1})$. Assume $s_1 \geq r$ in order to achieve the maximum order accuracy. We have:

$$\begin{aligned} e^{\lambda\omega} - 1 &= e^{\lambda(1-\delta)} - 1 = e^\lambda e^{-\lambda\delta} - 1 = e^\lambda e^{-\lambda\delta} - 1 = e^\lambda e^{-\lambda\delta} - e^\lambda + e^\lambda - 1 \\ &= (e^\lambda - 1) + e^\lambda(e^{-\lambda\delta} - 1). \end{aligned}$$

Therefore

$$\tilde{\omega} = \frac{(e^\lambda - 1) + e^\lambda(e^{-\lambda\delta} - 1)}{e^\lambda - 1} = 1 + \frac{e^\lambda}{e^\lambda - 1}(e^{-\lambda\delta} - 1).$$

On the other hand, using the Taylor expansion:

$$e^{-\lambda\delta} - 1 = \sum_{k=1}^{\infty} \frac{(-\lambda\delta)^k}{k!} = -\lambda\mathcal{O}(h^{s_1}).$$

Therefore

$$\tilde{\omega} = 1 - \frac{e^\lambda}{e^\lambda - 1} \lambda \mathcal{O}(\Delta x^{s_1})$$

and the desired accuracy is attained provided that $0 \ll \lambda = \mathcal{O}(1)$.

Figure 5 shows a plot of the mapping $\omega \rightarrow \tilde{\omega}$ for $\lambda = 14$.

4.5.2 Global average weight (GAW)

Using the weight defined through the smoothness indicator replacement in (4.5), a natural substitute of IS_{r_0} using every available r_0 -th order smoothness indicator is their harmonic mean:

$$IS_{r_0}^* := \frac{1}{\frac{1}{r-r_0+1} \sum_{j=0}^{r-r_0} \frac{1}{I_{r_0,j}}}.$$

We can thus define the new weight ω as

$$\omega := (1 - (1 - \rho)^{s_1})^{s_2},$$

where

$$\rho := \frac{IS_{r_0}^*}{I_r^*} = \frac{\frac{1}{\frac{1}{r-r_0+1} \sum_{j=0}^{r-r_0} \frac{1}{I_{r_0,j}^m}}}{\frac{1}{r-r_0+1} \sum_{j=0}^{r-r_0} I_{r_0,j}^m} = \frac{(r-r_0+1)^2}{\left(\sum_{j=0}^{r-r_0} I_{r_0,j}^m\right) \left(\sum_{j=0}^{r-r_0} \frac{1}{I_{r_0,j}^m}\right)},$$

and m is a parameter that enforces the convergence to 0 of the weight in a discontinuity. We next show that $0 \leq \rho \leq 1$ (and therefore ω verifies this property as well) as well as the desired properties both in smooth and non-smooth cases.

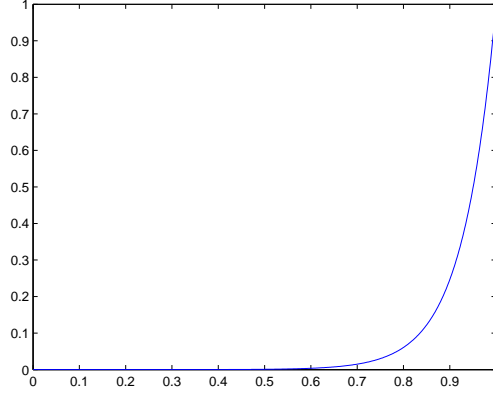


Fig. 5: Plot of the mapping $\omega \rightarrow \tilde{\omega}$ for $\lambda = 14$.

Property 2 $0 \leq \rho \leq 1$ and verifies

$$\rho = \begin{cases} 1 - \mathcal{O}(\Delta x^{2c_s}) & \text{if the stencil is } C^{r_0} \text{ with a } s\text{-th order zero derivative,} \\ \mathcal{O}(\Delta x^{2ms}) & \text{if the stencil contains a discontinuity,} \end{cases}$$

with $c_s := \max\{r_0 - s, 0\}$. Therefore

$$\omega = \begin{cases} 1 - \mathcal{O}(\Delta x^{2s_1c_s}) & \text{if the stencil is } C^{r_0} \text{ with a } s\text{-th order zero derivative,} \\ \mathcal{O}(\Delta x^{2s_2ms}) & \text{if the stencil contains a discontinuity.} \end{cases}$$

Proof Let $a_j > 0$, $1 \leq j \leq k$. We show that the quotient between their harmonic mean and their mean is bounded by 1, that is

$$0 \leq \rho = \frac{\frac{1}{\frac{1}{k} \sum_{j=1}^k \frac{1}{a_j}}}{\frac{1}{k} \sum_{j=1}^k a_j} \leq 1.$$

Since

$$\rho = \frac{\frac{1}{\frac{1}{k} \sum_{j=1}^k \frac{1}{a_j}}}{\frac{1}{k} \sum_{j=1}^k a_j} = \frac{k^2}{\left(\sum_{j=1}^k \frac{1}{a_j}\right) \left(\sum_{j=1}^k a_j\right)}$$

it suffices to show that

$$A := \left(\sum_{j=1}^k \frac{1}{a_j}\right) \left(\sum_{j=1}^k a_j\right) \geq k^2.$$

Indeed,

$$\begin{aligned} A &= \sum_{i=1}^k \sum_{j=1}^k \frac{a_i}{a_j} = k + \sum_{i=1}^k \sum_{j=1}^{i-1} \left(\frac{a_i}{a_j} + \frac{a_j}{a_i}\right) = k + \sum_{i=1}^k \sum_{j=1}^{i-1} \frac{(a_i - a_j)^2 + 2a_i a_j}{a_i a_j} \\ &= k + 2 \sum_{i=1}^k (i-1) + \sum_{i=1}^k \sum_{j=1}^{i-1} \frac{(a_i - a_j)^2}{a_i a_j} = k^2 + \sum_{i=1}^k \sum_{j=1}^{i-1} \frac{(a_i - a_j)^2}{a_i a_j} \geq k^2. \end{aligned}$$

Let us now assume that the stencil is C^{r_0} smooth with a s -th zero in the derivative, then

$$I_{r_0,j} = \Delta x^{2s} (1 + \mathcal{O}(\Delta x^{\max\{r-s,0\}})) = \Delta x^{2s} C(1 + \mathcal{O}(\Delta x^{c_s})).$$

Since we have actually proven that

$$A = k^2 + \sum_{i=1}^k \sum_{j=1}^{i-1} \frac{(a_i - a_j)^2}{a_i a_j},$$

replacing the a terms with the corresponding smoothness indicators to the power of m in case of smoothness

$$I_{r_0,j}^m = \Delta x^{2ms} C^m (1 + \mathcal{O}(\Delta x^{c_s}))^m = \Delta x^{2ms} C^m (1 + \mathcal{O}(\Delta x^{c_s})),$$

we have, denoting $k := r - r_0 + 1$,

$$\begin{aligned} A &= k^2 + \sum_{i=1}^k \sum_{j=1}^{i-1} \frac{(\Delta x^{2ms} C^m (1 + \mathcal{O}(\Delta x^{c_s})) - \Delta x^{2ms} C^m (1 + \mathcal{O}(\Delta x^{c_s})))^2}{\Delta x^{4ms} C^{2m} (1 + \mathcal{O}(\Delta x^{c_s}))^2} \\ &= k^2 + \sum_{i=1}^k \sum_{j=1}^{i-1} \frac{\Delta x^{4ms} C^{2m} (\mathcal{O}(\Delta x^{c_s}))^2}{\Delta x^{4ms} C^{2m} (1 + \mathcal{O}(\Delta x^{c_s}))} = k^2 + \sum_{i=1}^k \sum_{j=1}^{i-1} \frac{\mathcal{O}(\Delta x^{2c_s})}{1 + \mathcal{O}(\Delta x^{c_s})} \\ &= k^2 + \mathcal{O}(\Delta x^{2c_s}). \end{aligned}$$

Therefore,

$$\rho = \frac{k^2}{A} = \frac{k^2}{k^2 + \mathcal{O}(\Delta x^{2c_s})} = 1 + \mathcal{O}(\Delta x^{2c_s}).$$

Finally, if there is smoothness at least in one substencil with corresponding smoothness indicator $I_{r_0,i_0} = \Delta x^{2s} C(1 + \mathcal{O}(\Delta x^{c_s})) = \mathcal{O}(\Delta x^{2s})$ and a discontinuity crosses the stencil then there will be another substencil such that its smoothness indicator verifies $I_{r_0,j_0} = \mathcal{O}(1)$. Then, the corresponding term in the above sum (swapping the indexes if necessary, that is, if $i_0 < j_0$):

$$\frac{(I_{r_0,i_0}^m - I_{r_0,j_0}^m)^2}{I_{r_0,i_0}^m I_{r_0,j_0}^m} = \frac{(\mathcal{O}(\Delta x^{2ms}) - \mathcal{O}(1))^2}{\mathcal{O}(\Delta x^{2ms}) \mathcal{O}(1)} = \frac{\mathcal{O}(1)}{\mathcal{O}(\Delta x^{2ms})} = \mathcal{O}(\Delta x^{-2ms}),$$

and thus

$$A = \mathcal{O}(\Delta x^{-2ms}).$$

Therefore,

$$\rho = \frac{k^2}{A} = \frac{k^2}{\mathcal{O}(\Delta x^{-2ms})} = \mathcal{O}(\Delta x^{2ms}).$$

□

It follows from the result that to obtain an order of accuracy as large as possible, and if $r = 2r_0$, as it will be our usual choice of r_0 from now on, we must take $s_1 \geq r_0$ (to prevent from a possible extreme case $s = r_0 - 1$). Note that in the worst case scenario, $s \geq r_0$, implies an unavoidable downgrade of the accuracy as it happens with the original WENO-JS weights for reconstructions. The only way to overcome this issue is to add to each smoothness indicator the β defined above, but it will not be done in the forthcoming tests as we do not do it either in the definition of the WENO-JS weights in our numerical solver.

4.6 Weighted least squares extrapolation (WLS)

After some 2D order accuracy tests for smooth solutions with different spacing setups, it has been noticed that depending on the complexity of the domain, not only high order may not be achieved using straight Lagrange extrapolation at the ghost cells, but also the scheme might turn mildly unstable in some extreme cases, this independently of the choice for the spacing of the normal line points to be extrapolated at the ghost cell.

To avoid this phenomena, it is necessary to find an alternative to Lagrange (and weighted) extrapolation that stabilizes the scheme while keeping high order accuracy in terms of the global error. A possibility is to use least squares fitting as described in [12], [13].

Let $R \geq r$ and let $\{(x_i, u_i)\}_{i=0}^R$ be the stencil with nodal data, where $x_{i+1} - x_i = h$. Let us assume that we want to extrapolate or interpolate at the point x_* with a certain r -th degree polynomial

$$p(x) = \sum_{j=0}^r a_j x^j$$

using the data from the whole stencil. Since in general there is no polynomial of r passing through the R points, we find the polynomial $p(x)$ of degree r which minimizes the error with respect to $\{(x_i, u_i)\}_{i=0}^R$ in the L^2 -norm, i. e., we solve $p(x_i) = u_i$, $0 \leq i \leq R$ by least squares, which will be still a $(r + 1)$ -th order accurate approximation if the data is smooth.

We can now combine the least squares extrapolation, conceived for smooth regions with the already described techniques techniques based on weights. Let z_* be the result of the least squares extrapolation and v_* the result of some chosen modality of the weighted extrapolation techniques. To this aim we define a weight ω by using the information of the whole stencil of $R + 1$ points through the λ -UW or GAW technique and then take the final result of the extrapolation as

$$u_* := \omega z_* + (1 - \omega)v_*. \quad (7)$$

The simplest and most robust case for the election of v_* is to take $v_* = u_{i_0}$. This is ultimately the technique that will be used both for smooth and non-smooth problems in our numerical experiments, so that we will indicate by WLS-X the weighted least squares method with ω in (7) computed through the method X.

We next show a step-by-step algorithm of the chosen WLS-GAW technique, for a stencil $\{x_i\}_{i=0}^R$ with nodal values $\{u_i\}_{i=0}^R$, to be extrapolated at the point x_* , is thus:

1. Find the index $0 \leq i_0 \leq R$ such that x_{i_0} is the closest point to x_* . Then u_{i_0} is the reference value.
2. Compute the least-square polynomial of degree r at x_* , $p(x_*)$, using the whole stencil data.
3. Obtain the corresponding smoothness indicators from the substencils of size r_0 .
4. Compute the global average weight, w from the previously computed smoothness indicators.

5. The final extrapolated value, u_* , is then obtained as a weighted average of the least-square polynomial and the reference value, namely:

$$u_* = \omega p(x_*) + (1 - \omega)u_{i_0}.$$

We next summarize all parameters related to the size of the various stencils involved in the extrapolation:

- $r + 1$: Stencil size for Lagrange extrapolation. The accuracy order is thus $r + 1$ in case of smoothness.
- $r_0 + 1$: Substencil size used in the computation of the smoothness indicators.
- $R + 1$: Stencil size for least-squares extrapolation. In this context, we refer to r as the degree of the computed polynomial (hence the accuracy order is $r + 1$ as well).

Table 5 shows all the parameters involved in the different weight designs and indications on whether a parameter is involved or not on a particular method.

Method (columns) / Parameter (rows)	SW	IW	UW	GAW
s_1 : $\omega = \mathcal{O}(h^{\xi s_1})$ if discontinuity	Y	N	Y	Y
s_2 : $\omega = 1 - \mathcal{O}(h^{\xi s_2})$ if smoothness	Y	N	Y	Y
d : $\omega = \mathcal{O}(h^{\xi d})$ if discontinuity $\omega = 1 - \mathcal{O}(h^{\xi d})$ if smoothness	N	Y	N	N
λ : $\omega \rightarrow 0$ if $\lambda \rightarrow +\infty$ $\omega \rightarrow 1$ if $\lambda \rightarrow -\infty$	N	N	O	N
m : $\omega = \mathcal{O}(h^{\xi m})$ if discontinuity	N	N	N	Y

Table 5: List of parameters for the weights (Y: yes, N: no, O: optional). In each case, ξ is a parameter that depends on the method, the substencils size r_0 , the number of consecutive zero-derivatives and other parameters.

In the experiments in Section 5 the parameters are set to $R = 8$ (a stencil of 9 nodes to perform a least squares extrapolation), $r = 4$ (degree of the least squares interpolating polynomial), $r_0 = 2$ (substencils of size 3 where smoothness indicators are computed), $s_1 = r_0 = 2$ (requirement to match the whole scheme accuracy at the boundary provided that the first and second derivatives do not vanish simultaneously), $s_2 = 1$ and $m = 2$ (in order to mimic the exponent choice at the WENO-JS weights computation for spatial biased reconstructions, although in the boundary case it does not affect the order of the extrapolation when a discontinuity crosses the stencil since the alternative choice is just the constant extrapolation).

5 Numerical experiments

5.1 One-dimensional experiments

In this section we present some one-dimensional numerical experiments where both the accuracy of the extrapolation method for smooth solutions and its behavior in presence of discontinuities will be tested and analyzed.

5.1.1 Linear advection, C^∞ solution.

In this experiment we illustrate the performance of the proposed extrapolation method for a smooth solution. The problem statement for this test is the same as in [12]. We consider the following problem for the linear advection equation

$$\begin{cases} u_t + u_x = 0, & (x, t) \in (-1, 1) \times \mathbb{R}^+, \\ u(x, 0) = 0.25 + 0.5 \sin(\pi x), & x \in (-1, 1), \\ u(-1, t) = 0.25 - 0.5 \sin(\pi(1 + t)), & t \geq 0. \end{cases} \quad (8)$$

Outflow numerical boundary conditions are set at $x = 1$. The unique solution of this problem is

$$u(x, t) = 0.25 + 0.5 \sin(\pi(x - t)).$$

We perform tests at uniform meshes with resolutions given by $n = 20 \cdot 2^j$ points, $j = 1, \dots, 5$. As we use a fifth order accurate spatial scheme extrapolation is performed at 3 ghost cells at each side of the boundary. On the other hand, the time discretization is integrated with a third order method, hence we select a time step given by $\Delta t = \left(\frac{2}{n}\right)^{\frac{3}{5}}$, with corresponding Courant numbers $\Delta t/h_x = (2/n)^{2/3} \leq 1/20^{2/3}$ in order to attain fifth order accuracy in both integrators. Additionally, as the left boundary conditions are time dependent, a specific approximation is needed in each of the 3 stages of the RK3-TVD time integrator at the boundary in order not to lose accuracy, as indicated in [4]. The boundary values required in this case are the following:

- First stage: $g(t_k)$.
- Second stage: $g(t_k) + \Delta t g'(t_k)$.
- Third stage: $g(t_k) + \frac{1}{2} \Delta t g'(t_k) + \frac{1}{4} \Delta t^2 g''(t_k)$.

We run the simulation until $t = 1$ for all the previously specified resolutions and for different modalities of boundary extrapolation: IW, WLS-UW and WLS-GAW. We show the errors corresponding to 1- and ∞ -norm, and the numerical order computed from them in Tables 6–8.

n	Error $\ \cdot\ _1$	Order $\ \cdot\ _1$	Error $\ \cdot\ _\infty$	Order $\ \cdot\ _\infty$
40	8.73E-6	–	2.44E-5	–
80	2.70E-7	5.01	7.35E-7	5.05
160	8.45E-9	5.00	2.31E-8	4.99
320	2.64E-10	5.00	6.95E-10	5.06
640	8.26E-12	5.00	2.13E-11	5.03

Table 6: Error table for problem (8), $t = 1$, IW.

From the results, and comparing with those obtained in [1] it can be seen that IW behaves essentially as Lagrange extrapolation even for low resolutions, as it happens with thresholding extrapolation with not excessively restrictive parameter for the detection of discontinuities.

On the other hand, the two remaining techniques involving least squares extrapolation produce slightly less accurate results, but still fifth order accurate. This is what should be expected since a wider stencil is used, involving a polynomial

n	Error $\ \cdot\ _1$	Order $\ \cdot\ _1$	Error $\ \cdot\ _\infty$	Order $\ \cdot\ _\infty$
40	4.28E-5	–	1.99E-4	–
80	5.32E-7	6.33	1.86E-6	6.74
160	1.38E-8	5.26	4.65E-8	5.32
320	4.16E-10	5.06	1.43E-9	5.02
640	1.27E-11	5.03	4.49E-11	5.00

Table 7: Error table for problem (8), $t = 1$, WLS-UW.

n	Error $\ \cdot\ _1$	Order $\ \cdot\ _1$	Error $\ \cdot\ _\infty$	Order $\ \cdot\ _\infty$
40	1.50E-5	–	4.29E-5	–
80	4.56E-7	5.04	1.44E-6	4.90
160	1.37E-8	5.06	4.57E-8	4.98
320	4.16E-10	5.04	1.43E-9	5.00
640	1.27E-11	5.03	4.49E-11	4.99

Table 8: Error table for problem (8), $t = 1$, WLS-GAW.

of the same degree than IW. Albeit this fact, we will see in the next experiments that the WLS-X techniques are more robust than the ones based on Lagrange extrapolation for more demanding problems.

5.1.2 Burgers equation.

We now consider Burgers equation

$$u_t + \left(\frac{u^2}{2}\right)_x = 0, \quad \Omega = (-1, 1),$$

with initial condition $u(x, 0) = 0.25 + 0.5 \sin(\pi x)$, left inflow boundary condition given by $u(-1, t) = g(t)$ and outflow condition at the right boundary, where $g(t) = w(-1, t)$, with w the exact solution of the problem using periodic boundary conditions. Numerical errors for spatial resolutions $n = 40 \cdot 2^k$, $0 \leq k \leq 5$, corresponding to time $t = 0.3$ are presented in Tables 9-11. The solution is smooth and all methods provide fifth order accuracy as expected.

The conclusions for this test are the same than those drawn in the linear advection problem.

n	Error $\ \cdot\ _1$	Order $\ \cdot\ _1$	Error $\ \cdot\ _\infty$	Order $\ \cdot\ _\infty$
40	2.03E-5	–	3.57E-4	–
80	6.56E-7	4.95	1.47E-5	4.60
160	1.36E-8	5.59	2.81E-7	5.71
320	2.82E-10	5.58	9.16E-9	4.94
640	7.58E-12	5.22	2.76E-10	5.05
1280	2.23E-13	5.09	8.30E-12	5.06

Table 9: Error table for Burgers equation, $t = 0.3$. IW.

At further times a shock develops in the interior of the domain as shown in Figure 6a, corresponding to $t = 1.1$; at $t = 8$ the shock interacts with the inflow

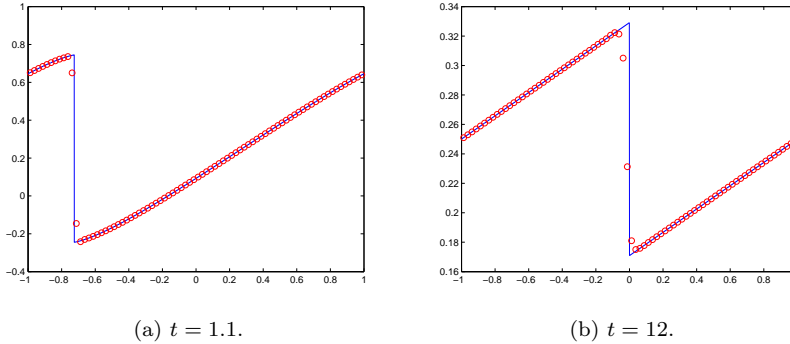
n	Error $\ \cdot\ _1$	Order $\ \cdot\ _1$	Error $\ \cdot\ _\infty$	Order $\ \cdot\ _\infty$
40	1.88E-3	—	3.65E-2	—
80	6.62E-5	4.82	3.94E-3	3.21
160	1.72E-7	8.52	9.45E-6	8.70
320	2.50E-9	6.10	9.45E-6	5.37
640	4.49E-11	5.80	6.73E-9	5.08
1280	9.61E-13	5.55	1.92E-10	5.13

Table 10: Error table for Burgers equation, $t = 0.3$. WLS-UW.

n	Error $\ \cdot\ _1$	Order $\ \cdot\ _1$	Error $\ \cdot\ _\infty$	Order $\ \cdot\ _\infty$
40	7.80E-4	—	2.61E-2	—
80	2.82E-6	8.11	8.14E-5	8.32
160	1.11E-7	4.66	6.31E-6	3.69
320	2.40E-9	5.53	2.28E-7	4.79
640	4.48E-11	5.74	6.73E-9	5.08
1280	9.61E-13	5.54	1.92E-10	5.13

Table 11: Error table for Burgers equation, $t = 0.3$. WLS-GAW.

boundary, being located at $x = 0$ at $t = 12$ as shown in Figure 6b. Both plots in Figure 6 illustrate that this discontinuity is properly captured by the scheme. Only the results for the WLS-GAW extrapolation method is included as the other methods provide similar results.

Fig. 6: Shock in Burgers equation, $n = 80$.

5.1.3 Euler equations.

The 1D Euler equations for gas dynamics are:

$$\begin{aligned}
 u_t + f(u)_x &= 0, \quad u = u(x, t), \quad \Omega = (0, 1), \\
 u &= \begin{bmatrix} \rho \\ \rho v \\ E \end{bmatrix}, \quad f(u) = \begin{bmatrix} \rho v \\ p + \rho v^2 \\ v(E + p) \end{bmatrix},
 \end{aligned} \tag{9}$$

where ρ is the density, v is the velocity and E is the specific energy of the system. The variable p stands for the pressure and is given by the equation of state:

$$p = (\gamma - 1) \left(E - \frac{1}{2} \rho v^2 \right),$$

where γ is the adiabatic constant, that will be taken as 1.4.

The initial data is the following, corresponding to the interaction of two blast waves:

$$u(x, 0) = \begin{cases} u_L & 0 < x < 0.1, \\ u_M & 0.1 < x < 0.9, \\ u_R & 0.9 < x < 1, \end{cases}$$

where $\rho_L = \rho_M = \rho_R = 1$, $v_L = v_M = v_R = 0$, $p_L = 10^3$, $p_M = 10^{-2}$, $p_R = 10^2$. Reflecting boundary conditions are set at $x = 0$ and $x = 1$, simulating a solid wall at both sides. This problem involves multiple reflections of shocks and rarefactions off the walls and many interactions of waves inside the domain. We will use the same node setup as in the previous tests.

Figure 7 shows the density profile at $t = 0.038$ at two different resolutions, being the reference solution computed at a resolution of $\Delta x = 1/16000$. The figure clearly shows that the results are satisfactory. The plot corresponds to the WLS-GAW method being the results obtained with the other methods almost identical

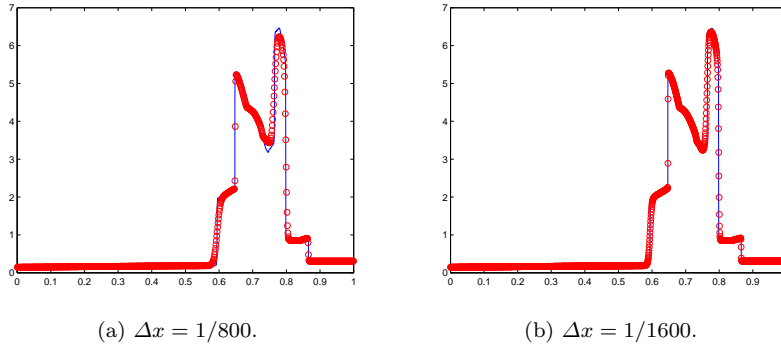


Fig. 7: Density profile, $t = 0.038$, WLS-GAW extrapolation.

5.2 Two-dimensional experiments

5.2.1 2D linear advection, C^∞ solution.

We consider the 2D linear advection equation

$$u_t + u_x + u_y = 0, \tag{10}$$

with

$$u_0 = u(x, y, 0) = 0.25 + 0.5 \sin(\pi(x + y)) \tag{11}$$

for different domains Ω . We start with a square, $\Omega = (-1, 1)$ where inflow conditions $g(t) = u(x, y, t) = 0.25 + 0.5 \sin(\pi(x + y - 2t))$ are imposed at the left and bottom boundary and outflow conditions at the rest. We compute the solution with the same setup and techniques to achieve fifth order accuracy as the above 1D tests for resolutions $n \times n$, for $n = 10 \cdot 2^j$, $1 \leq j \leq 6$, and we obtain the results in Tables 12-14 using different extrapolation techniques, running a simulation until $t = 1$.

n	Error $\ \cdot\ _1$	Order $\ \cdot\ _1$	Error $\ \cdot\ _\infty$	Order $\ \cdot\ _\infty$
20	5.36E-4	—	1.56E-3	—
40	1.66E-5	5.01	5.40E-5	4.85
80	5.24E-7	4.99	1.71E-6	4.98
160	1.65E-8	4.99	5.33E-8	5.00
320	5.15E-10	5.00	1.62E-9	5.04
640	1.63E-11	4.98	5.04E-11	5.01

Table 12: Error table for problem (10) - (11), Square domain, IW.

n	Error $\ \cdot\ _1$	Order $\ \cdot\ _1$	Error $\ \cdot\ _\infty$	Order $\ \cdot\ _\infty$
20	6.14E-3	—	9.07E-2	—
40	4.22E-5	7.19	2.98E-4	8.25
80	6.90E-7	5.93	3.47E-6	6.42
160	1.95E-8	5.15	9.13E-8	5.25
320	5.94E-10	5.04	2.81E-9	5.02
640	1.84E-11	5.01	8.90E-11	4.98

Table 13: Error table for problem (10) - (11), Square domain, WLS-UW.

n	Error $\ \cdot\ _1$	Order $\ \cdot\ _1$	Error $\ \cdot\ _\infty$	Order $\ \cdot\ _\infty$
20	8.22E-4	—	2.07E-3	—
40	2.12E-5	5.28	8.10E-5	4.68
80	6.39E-7	5.05	2.89E-6	4.81
160	1.94E-8	5.04	9.03E-8	5.00
320	5.94E-10	5.03	2.80E-9	5.01
640	1.84E-11	5.01	8.91E-11	4.98

Table 14: Error table for problem (10) - (11), Square domain, WLS-GAW.

We now change the domain and set Ω with respective boundary conditions as indicated in Figure 8.

This time, the complexity of the domain makes Lagrange extrapolation mildly unstable, whereas WLS is still stable and fifth order accurate as we can see numerically in Tables 15-16 that it is indeed achieved, running a simulation until $t = 0.85$.

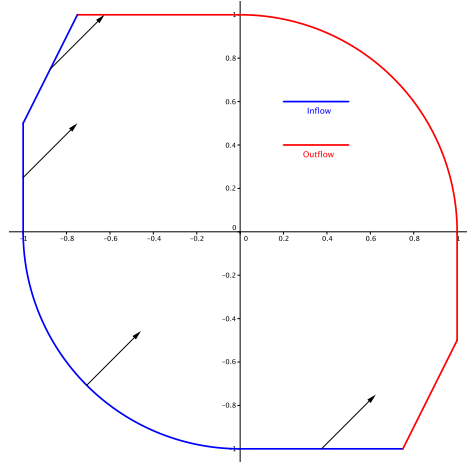


Fig. 8: Complex domain for 2D experiment.

n	Error $\ \cdot\ _1$	Order $\ \cdot\ _1$	Error $\ \cdot\ _\infty$	Order $\ \cdot\ _\infty$
20	1.14E-2	—	1.12E-1	—
40	4.82E-3	1.56	4.54E-2	1.40
80	8.33E-6	9.18	2.25E-4	7.66
160	7.53E-8	6.79	3.00E-6	6.23
320	2.14E-9	5.14	1.01E-7	4.89
640	6.59E-11	5.02	3.57E-9	4.82

Table 15: Error table for problem (10) - (11), Complex domain, WLS-UW.

n	Error $\ \cdot\ _1$	Order $\ \cdot\ _1$	Error $\ \cdot\ _\infty$	Order $\ \cdot\ _\infty$
20	3.78E-3	—	3.06E-2	—
40	8.04E-5	5.56	1.41E-3	4.44
80	1.81E-6	5.48	2.39E-5	5.88
160	6.81E-8	4.73	2.42E-6	3.31
320	2.13E-9	5.00	9.96E-8	4.60
640	6.58E-11	5.01	3.57E-9	4.80

Table 16: Error table for problem (10) - (11), Complex domain, WLS-GAW.

5.2.2 Euler equations.

The 2D Euler equations for inviscid gas dynamics are the following:

$$u_t + f(u)_x + g(u)_y = 0, \quad u = u(x, y, t),$$

$$u = \begin{bmatrix} \rho \\ \rho v^x \\ \rho v^y \\ E \end{bmatrix}, \quad f(u) = \begin{bmatrix} \rho v^x \\ p + \rho(v^x)^2 \\ \rho v^x v^y \\ v^x(E + p) \end{bmatrix}, \quad g(u) = \begin{bmatrix} \rho v^y \\ \rho v^x v^y \\ p + \rho(v^y)^2 \\ v^y(E + p) \end{bmatrix}. \quad (12)$$

In these equations, ρ is the density, (v^x, v^y) is the velocity and E is the specific energy of the system. The variable p stands for the pressure and is given by the

equation of state:

$$p = (\gamma - 1) \left(E - \frac{1}{2} \rho ((v^x)^2 + (v^y)^2) \right),$$

where γ is the adiabatic constant, that will be taken as 1.4 in all the experiments.

5.2.3 Double Mach Reflection

This experiment models a vertical right-going Mach 10 shock colliding with an equilateral triangle. By symmetry, we run the experiment in the upper half of the domain. The flow dynamics are driven by the Euler equations (12) and the initial conditions are the following:

$$u = (\rho, v^x, v^y, E) = \begin{cases} (8.0, 8.25, 0, 563.5) & \text{if } x \leq \hat{x}, \\ (1.4, 0, 0, 2.5) & \text{if } x > \hat{x} \end{cases}$$

where \hat{x} is the point where the ramp starts.

We run the simulation for $t = 0.2$. The experiment consists in several simulations using WLS both for GAW and for λ -UW for various values of λ . The results for two different resolutions are presented as Schlieren plots of the density field in Figures 9-10. The plots show the zone containing the complex shock reflection structure.

It can be seen at the figures that the performance of the new boundary extrapolation techniques are able to properly resolve the small-scale features present in this test for both methods, being the best results obtained with WLS-GAW and with WLS- λ -UW when taking the most negative values for λ . Let us recall that the scheme will tend to achieve higher order extrapolations at the boundary as $\lambda \rightarrow -\infty$.

On the other hand we report in Figures 9(a) and 10(a) results obtained using a first order extrapolation procedure (based on a one-node stencil). It can be appreciated that the high order extrapolation techniques indeed entail an improvement with respect to low order extrapolation, which illustrates the importance of keeping high order at the boundary even for scenarios where non-smooth structures appear.

5.2.4 Interaction of a shock with multiple circular obstacles

We now simulate a shock interacting with multiple solid circles. This test can also be found in [3], where penalization techniques were used to simulate problems including obstacles. In this case, we run the simulation until $t = 0.5$ and a mesh size of $h_x = h_y = \frac{1}{512}$ on the whole domain. In this case, the technique used for the numerical boundary conditions is WLS-GAW. As in the previous experiment, we present a Schlieren plot for the last time step in Figure 11. These results are consistent with those obtained in [3]. The result obtained in this experiment is very similar to the one obtained through the thresholding technique in [1]. The main difference is that this time a thresholding parameter is no longer needed, which is an advantage because in the case of thresholding extrapolation the performance of this problem was strongly dependent on the choice of the parameter, with moderate values leading to simulation failure and requiring very high values in order to get satisfactory results.

5.2.5 Steady-state supersonic flow around a triangle

We next simulate the flow field over a solid triangle with height $h = 0.5$ and half angle $\theta = 20$ deg moving at supersonic speeds. The initial conditions are

$$u = (\rho, v^x, v^y, p) = (1, \sqrt{\gamma}M_1, 0, 1)$$

and the computation is stopped when a steady state is obtained from the position of the shock waves. In order to halve the computational cost, we perform the simulation in the upper half of the domain, imposing appropriate reflecting boundary conditions at the symmetry axis. We solve this problem using the WLS-GAW technique at the boundary, as done in the previous experiment.

Figure 12 shows results that are consistent with those obtained in [3] and have sharper resolution than the ones reported in that paper for the same resolution.

6 Conclusions and future work

In this paper we have introduced some possible weighted extrapolations akin to WENO reconstructions capable of keeping high order accuracy for the global scheme, which entails an improvement with respect to the techniques based on thresholding parameters presented in [1]. On the other hand, as stated in [12], straight Lagrange extrapolation may lead to a mildly unstable scheme for multi-dimensional problems with some complex domains.

We have seen that an appropriate and efficient option to achieve good results both on smooth and non-smooth problems is to combine least squares with an unique weight design to reduce to the constant extrapolation (copying the value of the closest node) if there is a discontinuity in the extrapolation stencil. The results obtained with that technique are satisfactory and robust, with a weight design that, unlike those defined in [12], is dimensionless and scale independent.

From the experiments, it can be concluded that the WLS-GAW technique is better than WLS-UW without having to be scaled artificially (“magnetize” the weights to 1) in order to obtain a less diffusive profile. We have seen that the results of WLS-GAW are better than WLS-UW even for quite negative λ values.

Since we now have a fully developed boundary extrapolation strategy, our next purpose is to develop a parallelized AMR code [2], exploiting the main benefits of using this global scheme in the above terms. The extension of all the mentioned techniques to 3D is also under consideration.

References

1. Baeza, A., Mulet, P., Zorío, D.: High order boundary extrapolation technique for finite difference methods on complex domains with Cartesian meshes. *J. Sci. Comput.* **66**, 761–791 (2016).
2. Baeza, A., Mulet, P.: Adaptive mesh refinement techniques for high-order shock capturing schemes for multi-dimensional hydrodynamic simulations. *Int. J. Numer. Meth. Fluids* **52**, 455–471 (2006)
3. Boiron, O., Chiavassa, G., Donat, R.: A high-resolution penalization method for large Mach number flows in the presence of obstacles. *Computers & Fluids* **38**, 703–714 (2009).

4. Carpenter, M., Gottlieb, D., Abarbanel, S., Don, W.S.: The theoretical accuracy of Runge-Kutta time discretizations for the initial boundary value problem: a study of the boundary error. *SIAM J. Sci. Comput.* **16**, 1241–1252 (1995)
5. Donat, R., Marquina, A.: Capturing shock reflections: An improved flux formula. *J. Comput. Phys.* **125**, 42–58 (1996)
6. Filbert, F., Yang, C.: Inverse Lax-Wendroff method for boundary conditions of Boltzmann type models. *J. Comput. Phys.* **245**, 43–61 (2013)
7. Jiang, G.S., Shu, C.W.: Efficient implementation of Weighted ENO schemes. *J. Comput. Phys.* **126**, 202–228 (1996)
8. Marquina, A., Mulet, P.: A flux-split algorithm applied to conservative models for multi-component compressible flows. *J. Comput. Phys.* **185**, 120–138 (2003)
9. Shu, C.W., Osher, S.: Efficient implementation of essentially non-oscillatory shock-capturing schemes. *J. Comput. Phys.* **77**, 439–471 (1988)
10. Shu, C.W., Osher, S.: Efficient implementation of essentially non-oscillatory shock-capturing schemes, II. *J. Comput. Phys.* **83**(1), 32–78 (1989)
11. Sjogreen, B., Petersson, N.: A Cartesian embedded boundary method for hyperbolic conservation laws. *Commun. Comput. Phys.* **2**, 1199–1219 (2007)
12. Tan, S., Shu, C.W.: Inverse Lax-Wendroff procedure for numerical boundary conditions of conservation laws. *J. Comput. Phys.* **229**, 8144–8166 (2010)
13. Tan, S., Wang, C., Shu, C.W., Ning, J.: Efficient implementation of high order inverse Lax-Wendroff boundary treatment for conservation laws. *J. Comput. Phys.* **231**(6), 2510–2527 (2012)

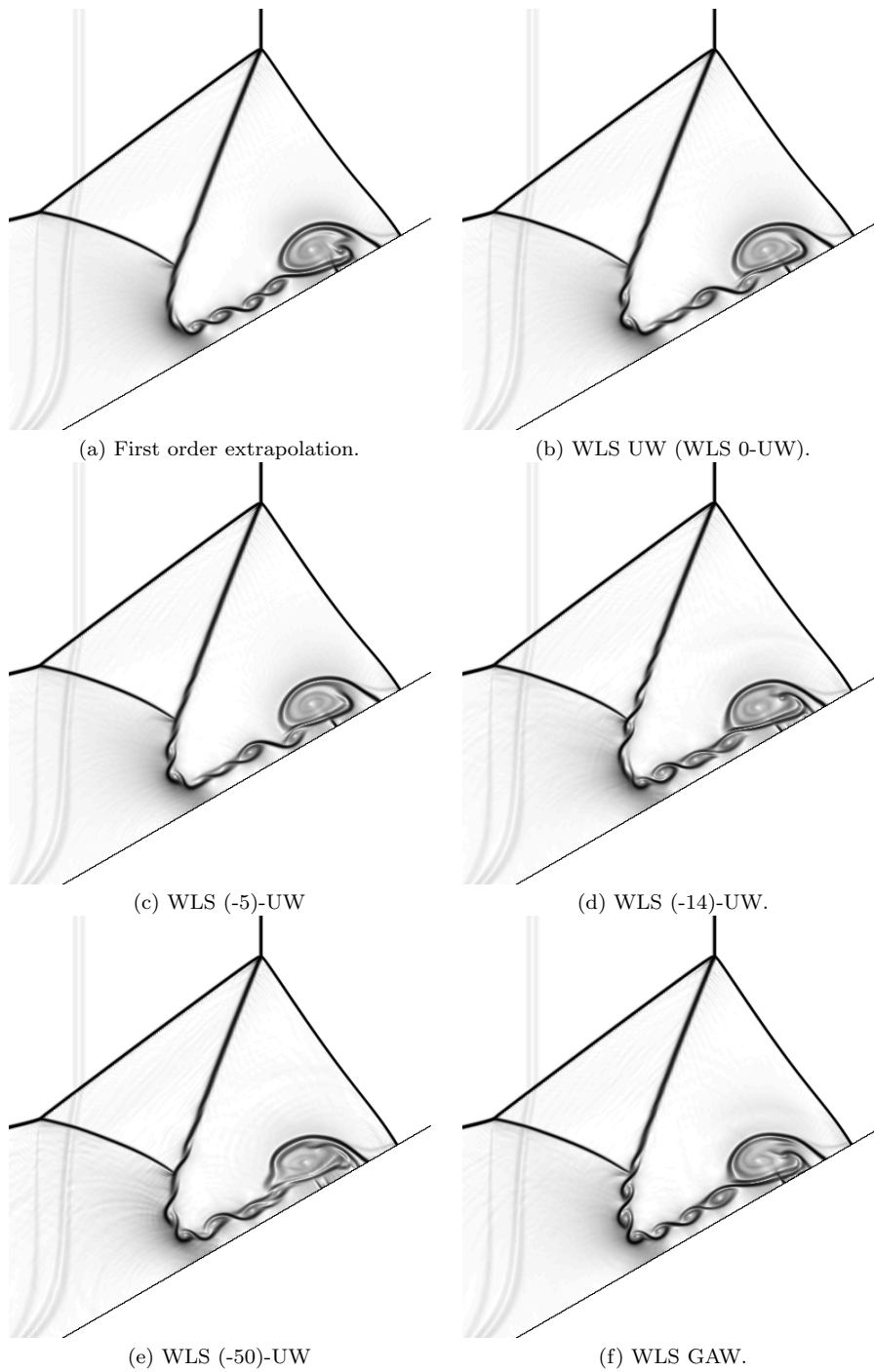


Fig. 9: Schlieren plots of the density for the Double Mach Reflection problem.

$$h_x = h_y = \frac{\sqrt{3}}{2} \frac{1}{512} \text{ (enlarged view)}$$

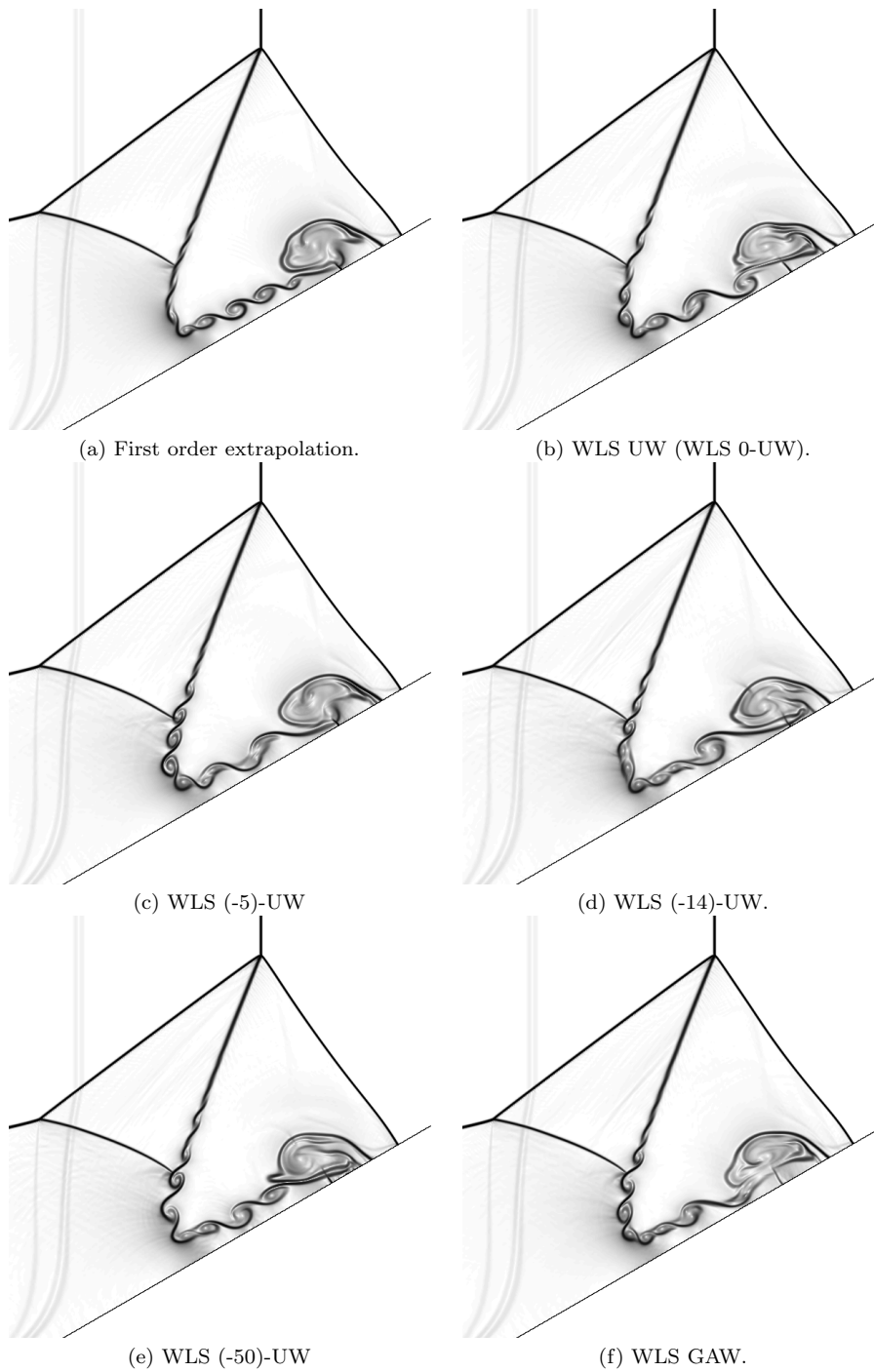


Fig. 10: Schlieren plots of the density for the Double Mach Reflection problem.

$$h_x = h_y = \frac{\sqrt{3}}{2} \frac{1}{640} \text{ (enlarged view)}$$

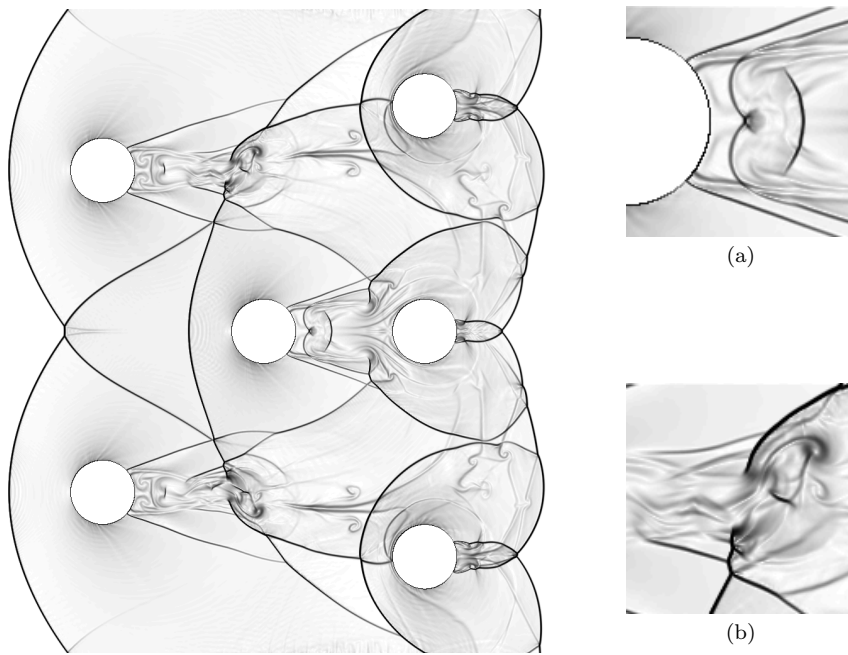


Fig. 11: Circles. (a) Central circle (enlarged view). (b) Turbulences aside upper-left circle (enlarged view).

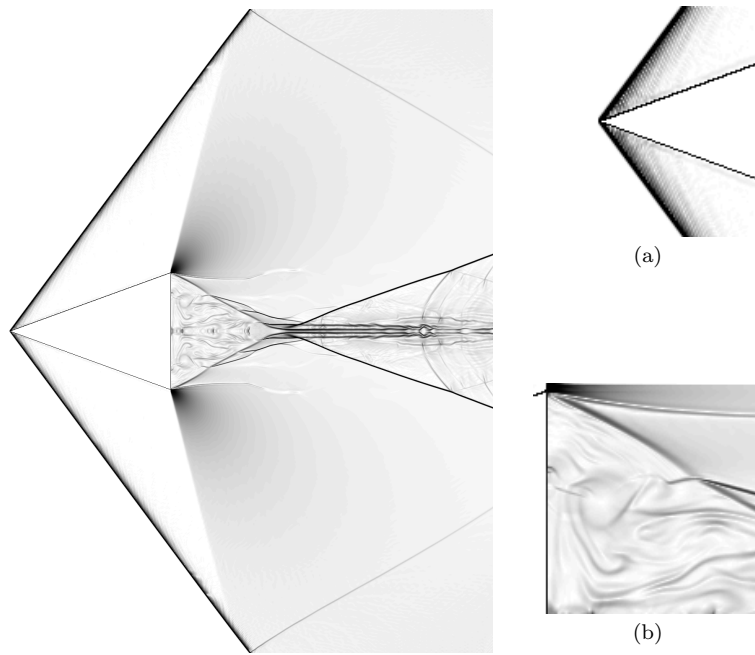


Fig. 12: Triangle. (a) Left wedge (enlarged view). (b) Turbulences aside upper right corner of the triangle (enlarged view).